

ROTORDYNAMIC STABILITY PROBLEMS AND SOLUTIONS IN HIGH PRESSURE TURBOCOMPRESSORS

J. Schmied
Sulzer Escher Wyss, Ltd.
Zurich, Switzerland

The stability of a high pressure compressor is investigated with special regard to the self-exciting effects in oil seals and labyrinths. It is shown how to stabilize a rotor in spite of these effects and even increase its stability with increasing pressure.

Notation

B	width of oil seals
d	damping coefficients of oil seals or labyrinths
D	modal damping factor
	shaft diameter
f	frequency in cps
F_d	displacement dependent oil film force
F_f	friction force
F^*	reference force for oil film forces (see equation (4))
i	imaginary unit, $i = \sqrt{-1}$
k	stiffness coefficient of oil seals or labyrinths
m	mass of oil seal rings
n	rotational speed
p	pressure
r	coordinate in radial direction
R	shaft radius
R_p	radius of the curvature of a pad
S_o	Sommerfeld number, $S_o = F_d/F^*$
w_{in}	inlet swirl velocity
w_{rot}	circumferential velocity of the shaft surface
α	real part of an eigenvalue
β	ratio of width to diameter
	dimensionless damping coefficient
γ	angle between displacement and displacement dependent oil film forces
δ	bearing clearance
	seal ring clearance
ϵ	dimensionless radial displacement, $\epsilon = 2r/\delta$
ϕ	circumferential coordinate

λ	eigenvalue, $\lambda = \alpha + i\nu$
ν	imaginary part of eigenvalue
η	oil viscosity
Ψ	relative clearance of oil seal ring
Ψ_b	relative bearing clearance
Ψ_p	relative pad clearance, $\Psi_p = (R_p - R)/R$
Ω	angular velocity of the rotor

Frequently used subscripts

x	subscript for x-direction (vertical)
y	subscript for y-direction (horizontal)
r	subscript for radial direction
ϕ	subscript for circumferential direction
1	subscript for the direction of the displacement dependent oil film force
2	subscript for the direction vertical to 1

1. Introduction

High pressure turbocompressors with a discharge pressure of 600 bar or more are very sensitive to instabilities because of the very high fluid forces in the seals. Often these compressors are used in offshore applications and therefore call for weight saving efforts like less casing per train hence more stages per rotor. This requires longer rotors, which make them even more sensitive to instabilities.

Well known destabilizing effects are

- Internal damping (shrink fit hysteresis, material damping).
- Oil whip in bearings.
- Oil whip in oil seals.
- Self-excitation due to the flow in labyrinths.

Internal damping is a source of self-excitation, if the compressor is run above its first critical speed, as high pressure compressors normally do. This effect, however, is probably the least important one of the above mentioned effects. Problems due to it can be avoided by a proper design (minimization of the friction in shrink fits).

Oil whip in bearings is prevented by using tilting pad bearings and therefore is not a real problem any more.

Oil seals for shaft end sealing are often designed as floating seal rings (fig. 3). The ring is pressed against the casing due to the pressure difference. The friction at the contact surface inhibits the radial floating motion. If the ring is blocked it affects the rotor quite similarly to a plain bearing, hence can cause oil whip at high rotational speeds (often at approximately twice the first critical speed). Special care has to be taken of this problem in case of high pressure differences (200 bar or more), since this calls for long rings causing high oil film forces and also increases the friction enhancing a blocking of the ring. The danger of blocking has to be prevented by pressure balancing the ring and thus reducing the friction force. If the friction, however, is too small the ring can become unstable.

The self-exciting effect of the flow in labyrinths on impeller shrouds, hubs and the balance piston is the most severe destabilizing effect. Without design features to reduce it a high pressure compressor normally can not be run. Swirl brakes for example are such a design feature. Combined with the proper choice of labyrinths they not only prevent an instability but even increase the stability with increasing pressure.

In this paper a high pressure compressor is demonstrated as an example of how to achieve a stable operation of the rotor. The destabilizing effects in the oil seals and labyrinths are handled in detail. It is also shown how to prevent an instability of the oil seal rings. The investigation is mainly carried out theoretically. The most important properties of the labyrinths, however, are checked by measured data.

2. Description of the investigated compressor rotor

The compressor we are dealing with in this paper was designed as a feasibility study for an offshore reinjection application. Figure 1 shows the rotor. It has eight stages with an intercooler after the fourth stage. The basic data are

Suction pressure	198 bar.
Discharge pressure	700 bar.
Molecular weight of the gas	20.05.
Mass flow	47.5 kg/s.
Rotor mass	265 kg.
Bearing distance	1565 mm.
Operating speed	13400 rpm.

The impeller has just a slight shrink fit for centering. The moment is mainly transmitted by dowel pins, which also position the impeller axially. Sleeves are therefore not necessary. This design minimizes the internal friction and allows a large shaft diameter, hence a stiff shaft.

The rotor is supported on two tilting pad bearings with four equal pads. The data of the two bearings are shown in table 1. The damping and stiffness coefficients as well as the oil viscosity are valid for operating conditions. The bearings are isotropic and have no cross coupling coefficients.

Figure 2 shows the modal damping factors D and the frequencies f of the first two bending modes (forward and backward whirl) of the rotor for different rotational speeds. They are determined from the eigenvalues $\lambda = \alpha \pm i\nu$ of a Finite Element model of the rotor as follows:

$$f = \nu / (2\pi) \quad (1)$$

and

$$D = -\alpha / |\lambda|. \quad (2)$$

The eigenvalue extraction was carried out with the program MADYN (ref.1). The oil film viscosity which might change in reality with the rotational speed is assumed to be constant in the calculation. The influence of the seals is not taken into account here. It will be considered later.

The rotational speeds in fig.2 at intersections of the line $f=n/60$ with the frequency curves are critical speeds. The first critical speed is at 3700 rpm. The corresponding damping factor is 15%. The critical speeds with the second bending modes have a very high damping (>30%). Resonances at these speeds therefore will hardly be detectable. The shown eigenvalues are approximately valid for running the rotor up and down, since the pressure in the compressor then is low. Under operating conditions however they change considerably because of the fluid forces in the seals, as we will see later in paragraph 5.

3. Description of the oil seals

Figure 3 shows the floating seal ring of the oil seals. In order to tighten the high pressure against atmospheric pressure the ring is pressed against the casing by an axial force resulting from the pressure difference and the surfaces on which the pressures act. The axial force must not be too small since contact between the ring and the casing must be guaranteed in spite of pressure fluctuations. However it should also not be too large because of the friction force inhibiting the radial motion of the ring.

Two extreme assumptions for the determination of the axial force can be made. The first is, that the outer edge of the contact surface tightens against the atmospheric pressure. This yields a maximum axial and friction force. Assuming that the inner edge tightens yields minimum forces. For our seal these forces are

Maximum axial force:	22267 N.
Minimum axial force:	4517 N.
Maximum friction force:	3565 N.
Minimum friction force:	570 N.

For the friction forces a friction coefficient of 0.16 is assumed.

A Finite Element calculation (results not shown here) considering the thermal deformation of the ring and the deformation due to the pressures showed that the first assumption yielding maximum forces seems to be more realistic.

For the linear rotordynamic calculations (see paragraph 5) we assume either ideally floating or locked up rings. Reality of course is between these two extreme cases.

For the ideally floating case we assume that the rings do not affect the rotor at all; that is, they are not modelled at all.

For the locked up case we assume a centered position of the ring relative to the static position of the shaft. This is realistic, since the compressor is run up with low pressure; hence the friction force is low during running up and the ring can center itself very well. This is in favor of a uniform gap, which prevents the surfaces in the gap to be damaged by small particles transported in the seal oil. The self-excitation, however, then becomes a maximum, if the ring is blocked due to the increased pressure.

For the latter case the oil seals are modelled by linear damping and stiffness coefficients in the same way as journal bearings. More accurately explained, they are considered as short, noncavitating journal bearings.

Our ring with a ratio of width to diameter of 0.35 can be considered as short. This allows us to neglect the pressure gradient in circumferential direction for small disturbances of the centered position. The coefficients then can be calculated analytically from the Reynolds equation (ref.2).

The bearing is considered as noncavitating, since the axial pressure drop normally suppresses any cavitation for small disturbances of the centered position.

The thus determined coefficients are

$$\begin{aligned} k_{xx} &= 0, \\ k_{xy} &= -k_{yx} = \beta^2 \pi F^* / \delta, \end{aligned} \quad (3)$$

$$\begin{aligned} dx &= dy = 2 \beta^2 \pi F^* / (\delta \Omega), \\ dxy &= 0, \end{aligned} \quad (4)$$

with

$$\beta = B / D \quad (5)$$

as the ratio of width to diameter and

$$F^* = D B \eta \Omega / \Psi^2 \quad (6)$$

as a reference force.

These coefficients are twice as large as those of a cavitating short bearing (ref.2). The data of the oil seals to determine the reference force are

width	B = 38.5 mm,
shaft diameter	D = 110.0 mm,
oil viscosity	$\eta = 0.015 \text{ Ns/m}^2$,
relative clearance	$\Psi = 1.36 \text{ ‰}$.

4. Description of the labyrinth seals

The investigation is carried out for the following labyrinth types on the shrouds, hubs and the balance piston.

Balance piston	: Comb grooved labyrinths.
Hub	: Straight-through labyrinths.
Impeller shrouds	: Straight-through, comb grooved labyrinths.

All labyrinths are stator labyrinths. Their geometry is shown in figure 4 a,b,c.

The gas data of each labyrinth are given in table 2. Data of the hub labyrinth of the eighth stage are not given, since the influence of this labyrinth is negligible compared to the influence of the labyrinth on the balance piston just following it.

The inlet swirl velocity of the fluid at each labyrinth is the main cause of the self-excitation of the rotor. It is zero for the hub labyrinths because of the diffuser and return

channel vanes. These labyrinths therefore rather have a damping than an exciting effect. For the other labyrinths the inlet swirl velocity is about 75% of the circumferential velocity of the rotor surface at the labyrinth inlet. When using swirl brakes it is only about 15% of the velocity of the rotor. These values were measured on a real compressor at high pressures at the author's company (ref.3).

The labyrinths are modelled by damping and stiffness coefficients just like the oil seals. These coefficients are calculated according to the theory of Wyssmann et al. (ref.4). Figure 5 shows thus calculated coefficients for the two types of shroud labyrinths of the sixth stage for two different inlet swirl velocities (with and without swirl brakes).

The cross coupling stiffness k_{xy} increases with increasing inlet swirl. The line for the comb grooved labyrinth is shifted to smaller values compared to the straight-through labyrinth. For small inlet swirls, k_{xy} even becomes negative. Therefore care must be taken concerning the excitation of backward whirling modes when using this labyrinth type.

The direct damping coefficient d_{xx} of the comb grooved labyrinth, hence its damping effect, is much smaller than the one of the straight-through labyrinth. For both labyrinths it almost does not depend on the inlet swirl. Due to this property it is possible to increase the stability of a compressor with increasing pressure. The exciting cross coupling stiffness increasing for higher pressures is reduced by swirl brakes, whereas the damping, which also increases for higher pressures, remains unaltered when reducing the swirl.

The ratio of k_{xy} to d_{xx} is considerably larger for the comb grooved labyrinth, except in the small region where k_{xy} is zero or almost zero. Increasing the damping of a rotor by an appropriate inlet swirl therefore seems to be easier when using straight-through labyrinths. When using the comb grooved type one has to realize an inlet swirl, where k_{xy} is almost exactly zero. This is practically impossible.

The direct stiffness k_{xx} for both labyrinth types has considerable negative values for high inlet swirl velocities. For the relative velocity of 0.75 the direct labyrinth stiffness (of one labyrinth!) is about 16% of the stiffness of the rigid supported shaft. The shaft stiffness hereby is defined as a force applied in the middle of the shaft divided by the deflection at the same location due to this force. It can therefore be expected that the direct labyrinth stiffness can significantly reduce the natural frequencies of the rotor.

The cross coupling damping d_{xy} is a conservative term and therefore neither has an exciting nor a damping effect. It influences the rotor in a similar way as gyroscopic terms.

In order to check the theory coefficients of a straight-through and comb grooved labyrinth were measured on the test stand of the Turbomachinery Laboratories at the Texas A & M University. The test stand is described in detail in reference 5. The geometries of the measured labyrinths are shown in fig.6. The tests were carried out with air against atmospheric pressure.

Figure 7 and 8 show measured coefficients for an inlet pressure of 3.08 bar and a rotational speed of 9500 rpm as a function of the inlet swirl velocity. For comparison

calculated coefficients for the test labyrinths are also shown. The measurements confirm the following properties of the calculated coefficients:

- The cross coupling stiffness almost linearly depends on the inlet swirl.
- The cross coupling stiffness of the comb grooved labyrinth is negative for small positive inlet swirls.
- The direct damping almost does not depend on the inlet swirl for the comb grooved labyrinth. For the straight through labyrinths this property is not confirmed as well. It was better confirmed in the measurements presented in reference 3.
- The direct damping for the comb grooved labyrinth is much smaller than for the straight through labyrinth.
- The direct stiffness is negative.

The experimental uncertainty indicated in the figures by the vertical lines is ± 3.5 kN/m for stiffness and ± 60 Ns/m for damping. Hence the coincidence is acceptable. The calculated direct damping values tend to be too small. This however is not so severe, since one is always on the safe side when assessing the stability with calculated damping values. The magnitude of the direct stiffness values also tend to too small values.

5. Stability of the rotor

The stability of the rotor considering the fluid forces in the oil and labyrinth seals is assessed by calculated complex eigenvalues $\lambda = \alpha \pm i\omega$ of the Finite Element model of the rotor, respectively the modal damping factors D (see equation (2)). A positive damping factor means the rotor is stable, whereas it is unstable for negative damping factors.

Figure 9 a and b shows the damping factor and the frequency of the first backward and forward whirling bending mode for ideally floating seal rings. They are shown for the two mentioned labyrinth types at the operating speed of 13400 rpm without labyrinth influence, a condition which is realized in practice for very low pressures, as well as with labyrinth influence for the full discharge pressure of 700 bar. One can recognize the tremendous influence of the labyrinths on the damping as well as on the frequencies.

It can be seen that the forward whirl becomes unstable with increasing pressure for both labyrinth types if no swirl brakes are used. When using swirl brakes and straight-through labyrinths the damping of the rotor is considerably increased with increasing pressure. However when swirl brakes are used in combination with comb grooved labyrinths the backward whirl becomes unstable. This is due to the negative cross coupling stiffness of this labyrinth type for small inlet swirls (fig. 5).

Figure 10 and 11 show results of the rotor with centrally blocked oil seal rings. The modes are quite different from those of the rotor with ideally floating seal rings.

In figure 10 damping factors and natural frequencies of the first four modes are shown as a function of the rotational speed without labyrinth influence ($p = 0$). This figure is shown for a better understanding of the behavior of the rotor with blocked seal rings, although in reality a blocking of the seal rings is not possible for low pressures, that is for rotor speeds below the operating speed.

It can be seen that the frequency of mode 1 and 2 almost linearly depend on the rotor speed. The slopes of the frequency curves hereby are about 0.5. This clearly indicates that these frequencies are determined by the oil whirl in the seals, which approximately has a frequency of half the rotational speed. Mode number 1 becomes unstable at 8000 rpm. This is about twice the critical speed f_{1c} of the rotor without seals (also see figure 2). The oil whirl here turns into the well known oil whip.

Figure 11 shows the influence of labyrinths on the eigenvalues of the four modes in figure 10 at the operating speed. Results are only shown for straight-through labyrinths since comb grooved labyrinths are not recommendable because of the results discussed in figure 9.

It can be seen that the labyrinths make the rotor more stable if swirl brakes are used. The rotor however still is slightly unstable. The seal rings therefore must be balanced at any rate in order to come closer to the behavior in figure 9.

6. Stability of the seal ring

If the friction force between casing and floating seal ring is reduced too much, the ring can become unstable. The corresponding mode can be calculated by modelling the rotor including unbound floating seal rings without friction forces. In this mode the rotor practically does not move and the ring describes a circular orbit around the center of the shaft.

In the following we will calculate limit cycles of this unstable motion taking into account the nonlinear friction forces and also considering the oil film forces as nonlinear, since the expected deflections are in the order of magnitude of the seal ring clearance. Since the rotor practically does not move we consider it as fixed.

The equations of motion of the ring in radial and circumferential direction are (fig.12)

$$m (\ddot{r} - r \dot{\phi}^2) = F_r, \quad (7)$$

$$m (2\dot{r}\dot{\phi} + r\ddot{\phi}) = F_{\phi}, \quad (8)$$

where F_r and F_{ϕ} are the forces on the ring in the radial and circumferential direction. These forces consist of the oil film force and the friction force. They may be written as follows:

$$F_r = F_{dr}(r) - d_{rr}(r)\dot{r} - d_{r\phi}(r)\dot{\phi}r - F_{fr}, \quad (9)$$

$$F_{\phi} = F_{d\phi}(r) - d_{\phi r}(r)\dot{r} - d_{\phi\phi}(r)\dot{\phi}r - F_{f\phi}, \quad (10)$$

where $F_{dr}, F_{d\phi}$ are the displacement dependent oil film forces,
 $d_{rr}\dot{r}, d_{r\phi}\dot{\phi}r, d_{\phi r}\dot{r}, d_{\phi\phi}\dot{\phi}r$ are the velocity dependent oil film forces
and $F_{fr}, F_{f\phi}$ are the friction forces.

To determine limit cycles (i. e. stationary solutions of equation (7) and (8)) one has

$$\dot{r} = \ddot{r} = \ddot{\phi} = 0, \quad (11)$$

$$F_{fr} = 0, \quad (12)$$

$$F_{f\phi} = F_f. \quad (13)$$

Substituting equation (11), (12), and (13) into equation (7), (8), (9) and (10) yields

$$mr\dot{\phi}^2 = -F_{dr}(r) + d_{r\phi}(r)\dot{\phi}r, \quad (14)$$

$$0 = F_{d\phi}(r) - d_{\phi\phi}(r)\dot{\phi}r - F_f. \quad (15)$$

The solution of $\dot{\phi}$ can be extracted from equation (15):

$$\dot{\phi} = \frac{F_f - F_{d\phi}(r)}{rd_{\phi\phi}(r)}. \quad (16)$$

Equation (16) introduced in equation (14) delivers a quadratic equation for F_f :

$$\frac{m}{r} \left[\frac{F_f - F_{d\phi}(r)}{d_{\phi\phi}(r)} \right]^2 + d_{r\phi}(r) \frac{F_f - F_{d\phi}(r)}{d_{\phi\phi}(r)} + F_{dr}(r) = 0. \quad (17)$$

The solution of this equation is

$$F_f = F_{d\phi}(r) - \frac{d_{r\phi}(r)r + \sqrt{(d_{r\phi}(r)r)^2 - 4mF_{dr}(r)r}}{2m} d_{\phi\phi}(r). \quad (18)$$

The second solution of equation (17) with a "-" instead the "+" before the square root in equation (18) physically makes no sense. Since $F_{dr}(r)$ is always negative (eq.(19)), the root is larger than $d_{r\phi}(r)r$. Hence a "-" sign would always yield a friction force larger than the oil film force $F_{d\phi}(r)$ and ϕ would become negative according to equation (16). This means it would have the same direction as the friction force, which is not possible, since the friction force is not the driving force of the motion.

The displacement dependent forces in equation (16) and (18) are (fig. 12)

$$F_{dr}(r) = -F_d(r) \cos \gamma(r), \quad (19)$$

$$F_{d\phi}(r) = F_d(r) \sin \gamma(r), \quad (20)$$

with

$$F_d(r) = F^* So(r), \quad (21)$$

where F^* is the reference force according to equation (6) in paragraph 3 and So is the Sommerfeld number.

The damping coefficients in equation (16) and (18) are

$$d_{r\phi}(r) = F^*/(\delta\Omega) (b_{22}\sin\gamma\cos\gamma - b_{21}\sin^2\gamma + b_{12}\cos^2\gamma - b_{11}\sin\gamma\cos\gamma) \quad (22)$$

$$d_{\phi\phi}(r) = F^*/(\delta\Omega) (b_{22}\cos^2\gamma - b_{21}\sin\gamma\cos\gamma - b_{12}\sin\gamma\cos\gamma + b_{11}\sin^2\gamma) \quad (23)$$

where β_{22} , β_{21} , β_{12} and β_{11} are dimensionless damping coefficients in the 1,2 coordinate system in figure 12.

The Sommerfeld number and the dimensionless damping coefficients are calculated numerically from the Reynolds equation. A analytical solution by neglecting the pressure gradient in circumferential direction as in paragraph 3 is not possible any more, because the motion of the ring is not only a small disturbance of the centered position.

Figure 13 shows the relative displacement $\varepsilon=2r/\delta$ of the ring and the angle γ for different Sommerfeld numbers. Fig 14 shows the dimensionless damping coefficients as a function of ε .

Figure 15 a,b show the curves of equilibrium points according to equation (18) and (16) calculated with the values in figure 13 and figure 14 for a mass of the ring of 5.135 kg. It can be seen in figure 15a, that for friction forces below the maximum force of about 2700 N exist two equilibrium points ε_1 and ε_2 . The first point ε_1 is unstable. For the friction force zero this already has been stated at the beginning of this paragraph. For higher friction forces this can be verified by numerically solving equations (7) and (8). The diagram in figure 15a therefore can be understood as follows. If for any reason ε becomes equal or larger than ε_1 the centrifugal force will make the ring snap through to ε_2 , where it describes a circular orbit with the eccentricity ε_2 and the frequency according to figure 15b.

If the frequency of this motion is close to a natural frequency of the rotor which is not damped too strong, the rotor vibration is affected by the ring motion. The frequency of the ring motion then can be seen in the spectrum of a rotor vibration probe.

If the friction force is larger than the maximum in figure 15a the ring cannot describe a nondecaying motion on its own, hence it will follow the shafts motion. The ring should therefore be balanced in such a way that the friction force is slightly above the maximum in figure 15a.

It must be mentioned however, that the equilibrium points are very sensitive to the bearing data which are calculated numerically and therefore must not correspond to a real situation. The deduced desired friction force therefore can only be understood as a rough estimation and has to be confirmed experimentally.

7. Conclusions

The stability of a high pressure compressor rotor was investigated with special regard to the self-excitation in the oil and labyrinth seals. The investigations were carried out theoretically. It was shown that both effects can easily destabilize the rotor, if they are not treated properly.

For the labyrinth coefficients, measurements were also considered. A comparison with calculated coefficients showed that a theoretical stability analysis is on the safe side, since

the calculated direct damping coefficients tend to be too low. . Hence the theory is a sound, practical approach.

The self-excitation in the oil seals designed as floating seal rings can be avoided by balancing the ring in order to reduce the friction between casing and ring and guarantee its floating. If the friction, however, is too small, the ring is excited by the oil film force to a circular motion around the center of the shaft. The minimum friction force to prevent this unwanted motion was deduced.

The self-excitation in the labyrinths can be reduced by swirl brakes. Since the swirl brakes practically do not influence the damping but only the exciting cross coupling stiffnesses the rotor can become even more stable with increasing pressure. To achieve this however the properties of the chosen labyrinth type have to be taken into account. It was shown that a comb grooved labyrinth which has only little damping and negative cross coupling stiffnesses for small inlet swirls destabilizes the first backward whirling bending mode when using swirl brakes. An increasing stability with increasing pressure was achieved when using straight-through labyrinths.

References

1. Klement, H.D.: MADYN - ein Programmsystem für die Maschinenberechnung. Unix mail 5 (1987) 1.
2. Cameron, A.: Basic lubrication theory. Longman, London 1970.
3. Wyssmann, H.R.: Rotor Stability of High Pressure Multistage Centrifugal Compressors. Proceedings of the Conference on Rotating Machinery Dynamics, Boston 1987-DE-Vol.2, Editors A. Muszynska and J.C. Simonis (Book No. H0400B).
4. Wyssmann, H.R., Pham, T.C. and R.J. Jenny: Prediction of Stiffness and Damping Coefficients for Centrifugal Compressor Labyrinth Seals. ASME Journal of Engineering for Gas Turbines and Power, Vol. 106, October 1984.
5. Childs, D.W. et. al.: Theory Versus Experiment for the Rotordynamic Coefficients of Annular Gas Seals. Part 1 - Test Facility and Apparatus. ASME Journal of Tribology, Vol. 108, July 1986.

Table 1Bearing data ($n = 13400$ rpm)

	bearing 1		bearing 2	
Diameter	0.1	m	0.1	m
Width	0.05	m	0.05	m
Relative bearing clearance Ψ_b	0.2	%	0.2	%
Relative pad clearance Ψ_p	0.4	%	0.4	%
Oil viscosity	0.01	Ns/m ²	0.01	Ns/m ²
Static load	1251	N	1349	N
Stiffness coefficient	$7.15 \cdot 10^7$	N/m	$7.23 \cdot 10^7$	N/m
Damping coefficient	$5.16 \cdot 10^4$	Ns/m	$5.19 \cdot 10^4$	Ns/m

Table 2

Gas data of the labyrinths

a) Balance piston

mean viscosity [10^{-4} Ns/m ²]	0.47
density before lab. [kg/m ³]	348
pressure before lab. [bar]	682
pressure after lab. [bar]	198

b) Hub

stage	1	2	3	4	5	6	7
mean viscosity [10^{-4} Ns/m ²]	0.26	0.28	0.30	0.32	0.41	0.43	0.45
density before lab. [kg/m ³]	236	250	262	318	325	332	339
pressure before lab. [bar]	253	311	371	429	496	570	639
pressure after lab. [bar]	239	297	356	419	479	551	618

c) Shroud

stage	1	2	3	4	5	6	7	8
mean viscosity [10^{-4} Ns/m ²]	0.26	0.28	0.30	0.32	0.41	0.43	0.45	0.47
density before lab. [kg/m ³]	239	253	264	275	330	337	342	348
pressure before lab. [bar]	239	297	356	419	479	551	618	682
pressure after lab. [bar]	198	253	311	371	429	496	570	633

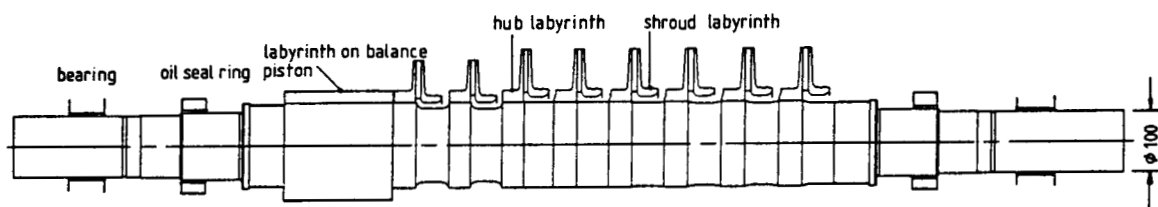


Fig.1 Investigated rotor

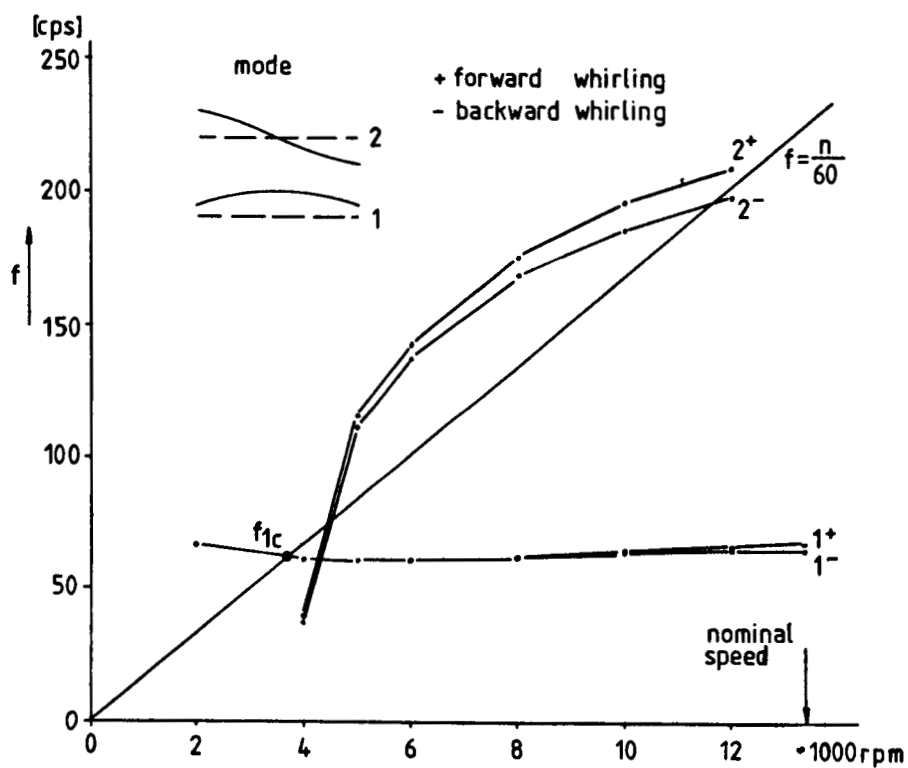
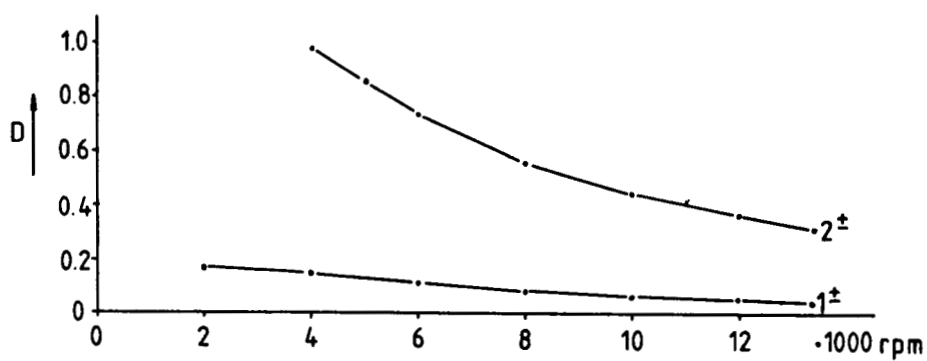


Fig.2 Modal damping factors and natural frequencies of the first two bending modes of the rotor

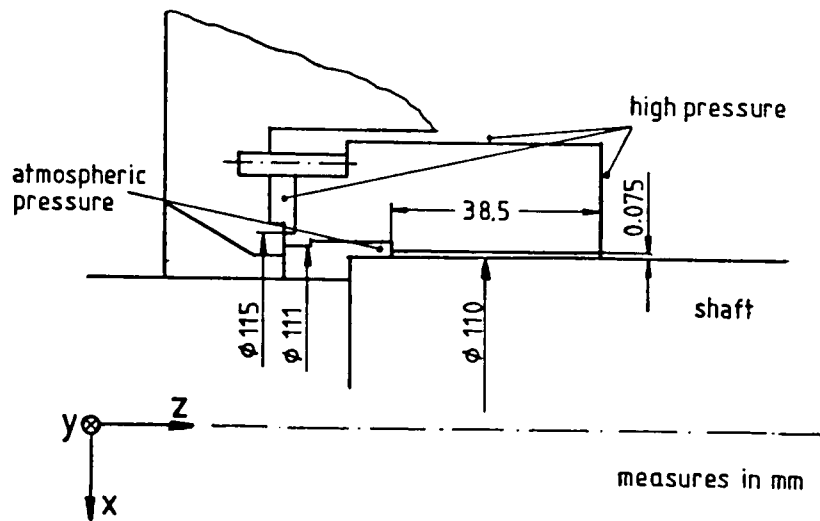
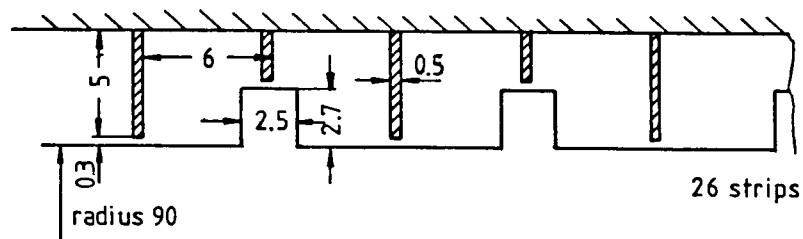
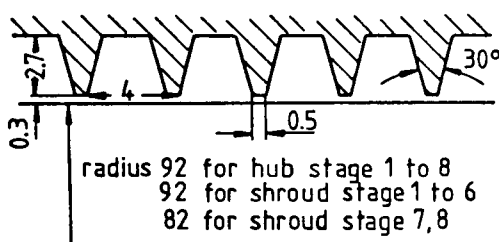


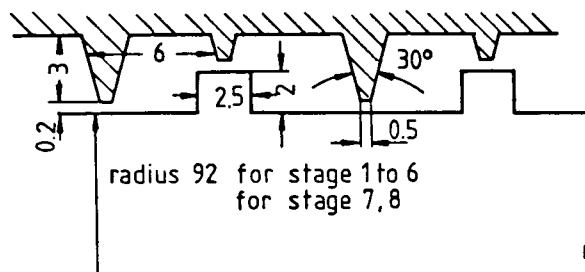
Fig.3 Floating seal ring



a) Balance piston



b) Hub and impeller shroud with straight-through labyrinth



c) Impeller shroud with comb grooved labyrinth

measures in mm

Fig.4 Geometry of labyrinths

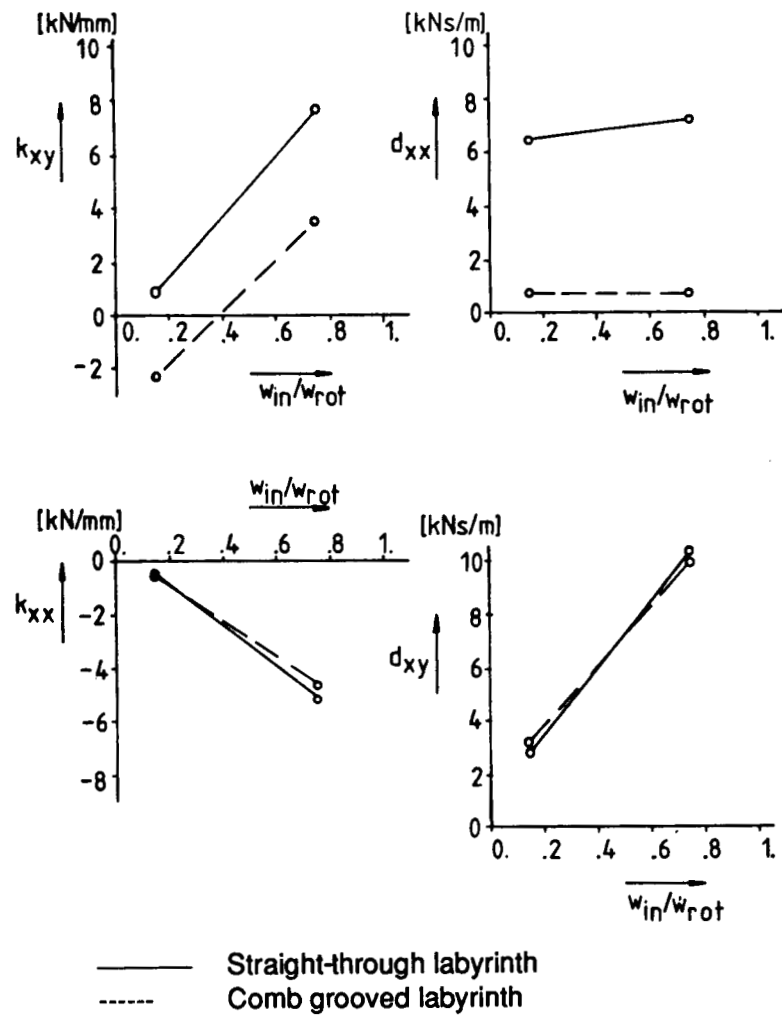


Fig.5 Calculated labyrinth coefficients with swirl brakes ($w_{in}/w_{rot}=0.75$) and without swirl brakes ($w_{in}/w_{rot}=0.15$)

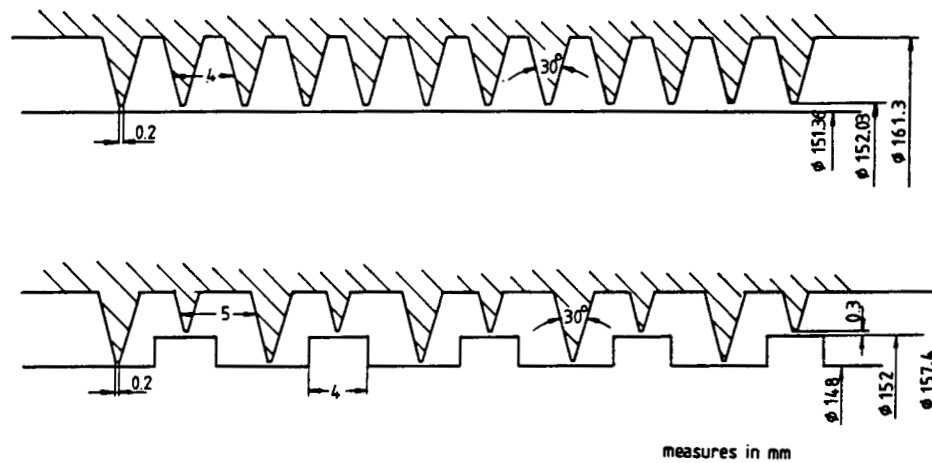


Fig.6 Geometry of measured labyrinths

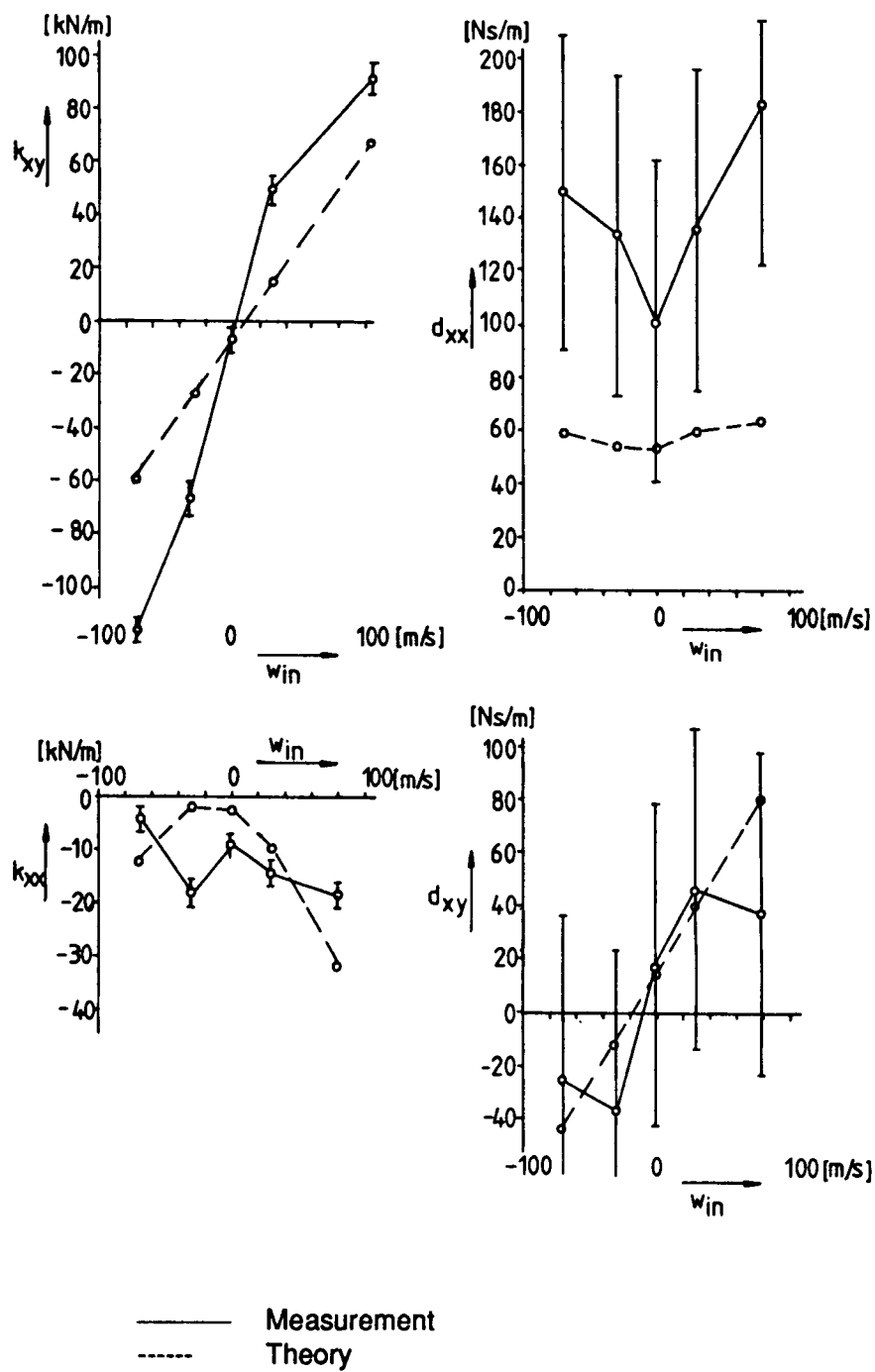


Fig.7 Comparison of measured and calculated coefficients for the straight-through labyrinth

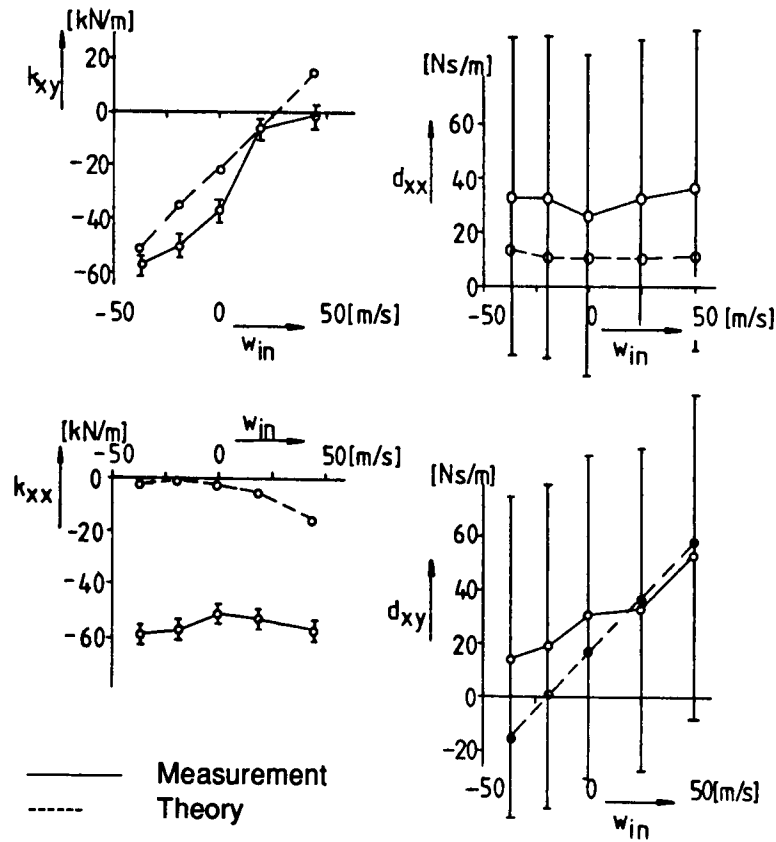


Fig.8 Comparison of measured and calculated coefficients for the comb grooved labyrinth

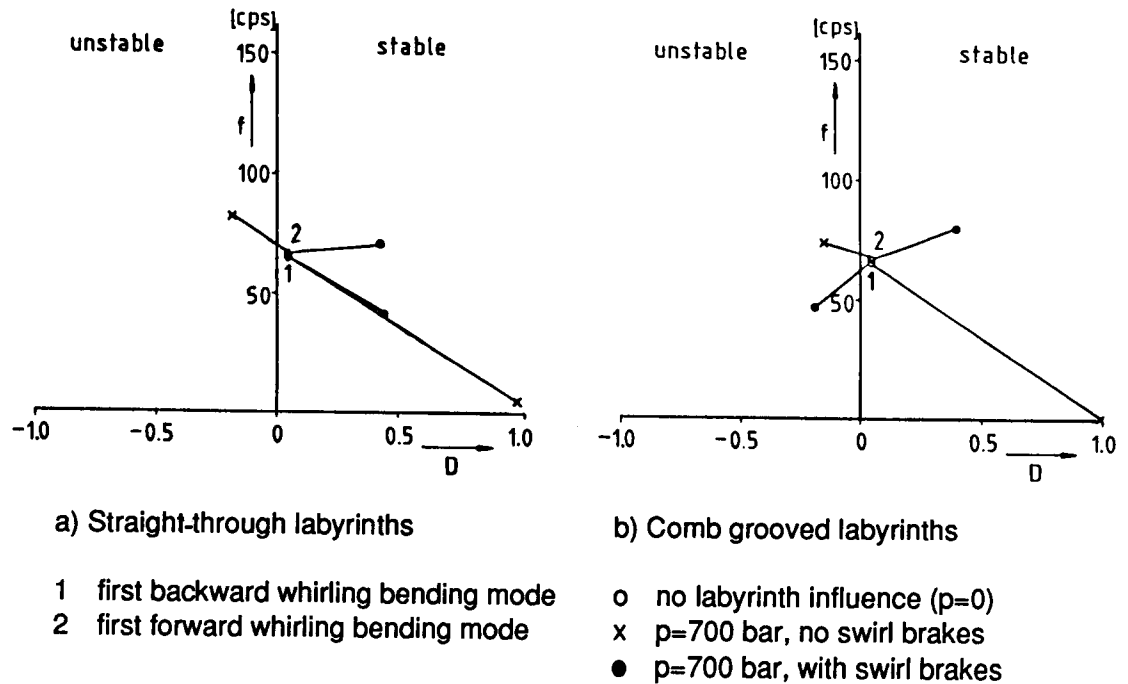


Fig.9 Influence of labyrinths on the damping factors and natural frequencies of the rotor with ideally floating oil seal rings. $n=13400$ rpm

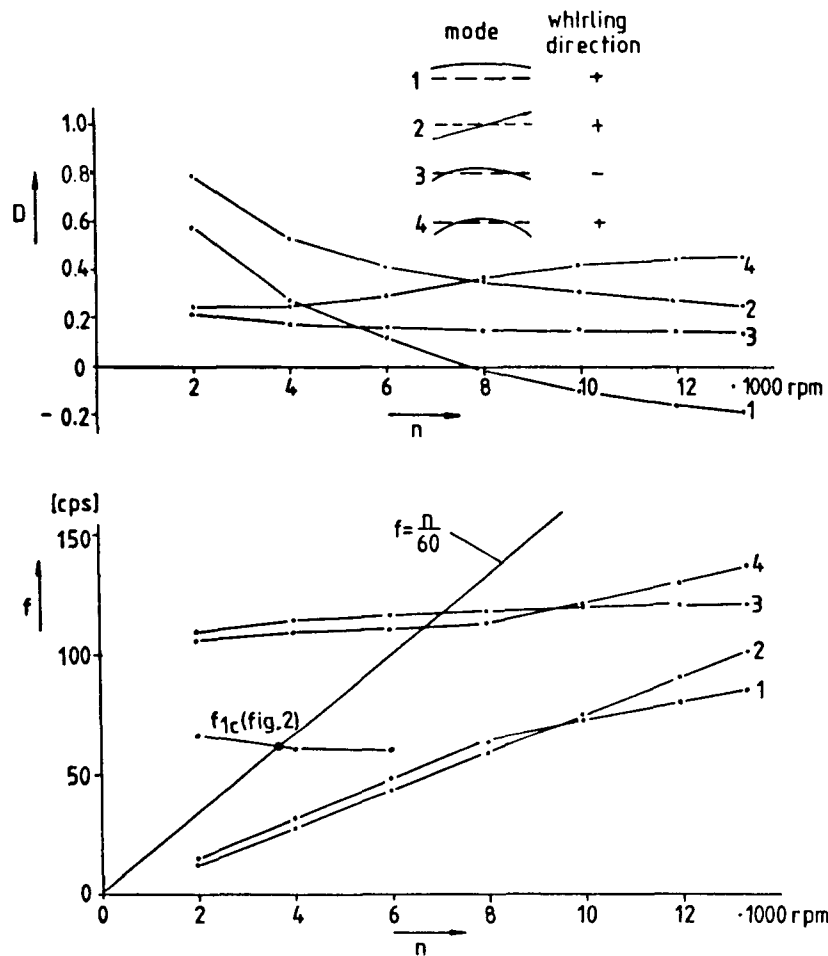


Fig.10

Damping factors and natural frequencies of the rotor for centrally blocked oil seals

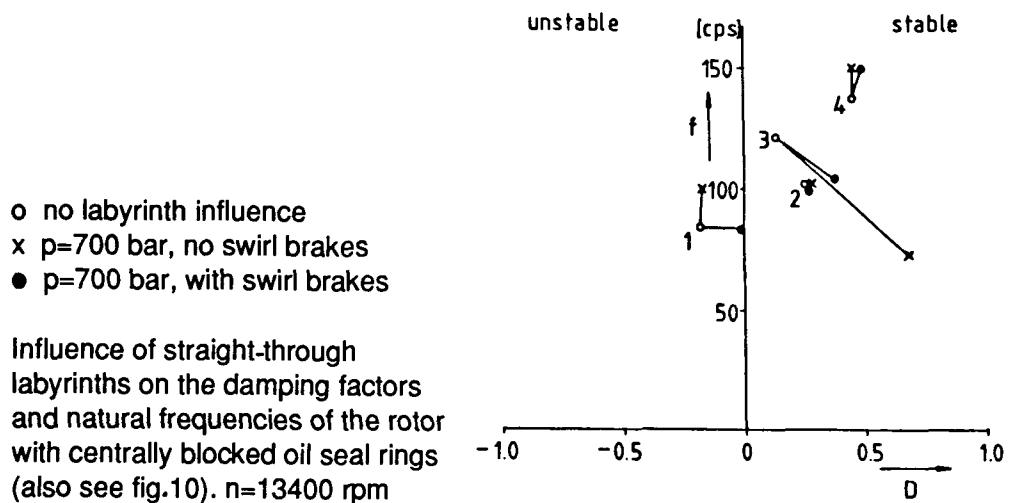


Fig.11

Influence of straight-through labyrinths on the damping factors and natural frequencies of the rotor with centrally blocked oil seal rings (also see fig.10). $n=13400$ rpm

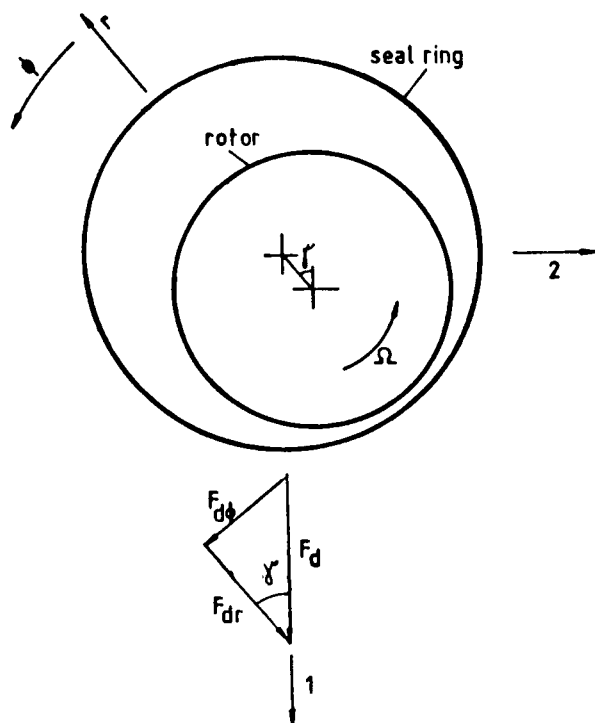


Fig.12 Coordinates to describe the ring motion and the forces on the ring

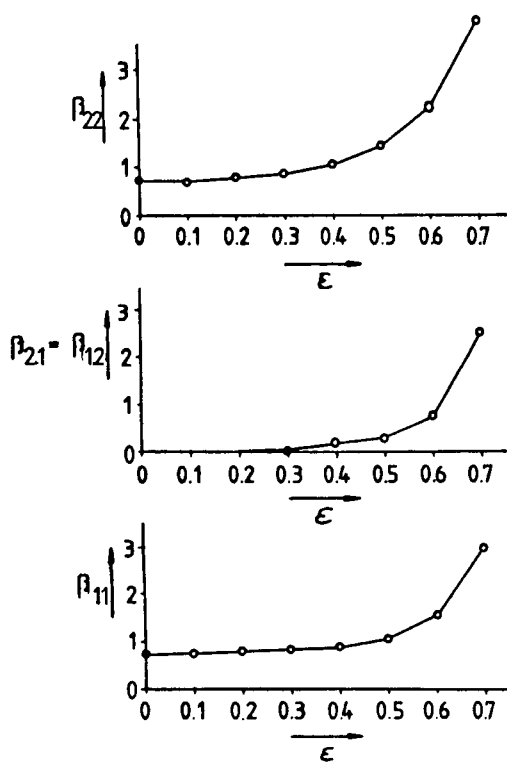


Fig.14 Dimensionless damping coefficients of the oil seal

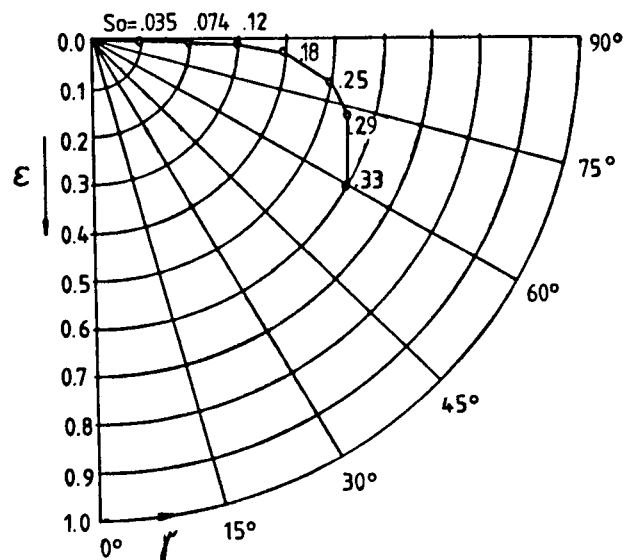
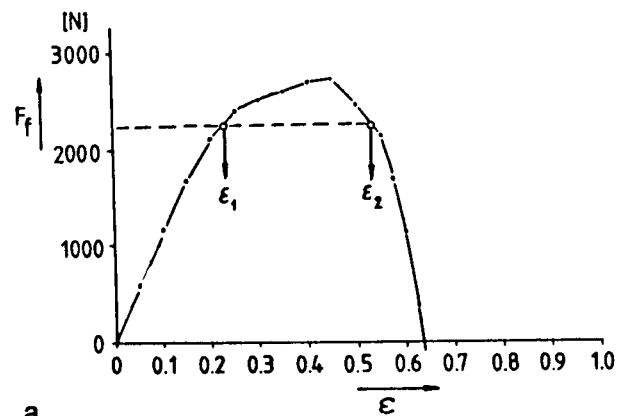
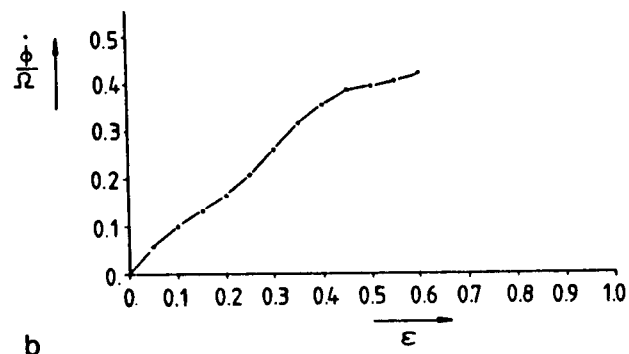


Fig.13 Relation between $\epsilon = 2r/\delta$, γ and So



a



b

Fig.15 Curves for the equilibrium of forces in radial and circumferential direction